ICARUS 73, 330–348 (1988)

On Disk–Planet Interactions and Orbital Eccentricities

WILLIAM R. WARD[1]

Geology and Planetology Section, Jet Propulsion Laboratory, California Institute of Technology, Pasadena, California 91109

Received December 18, 1986; revised July 27, 1987

The eccentricity evolution from density wave interaction between a planetesimal and a Keplerian disk is studied. While it is known that Lindblad resonances both interior and exterior to the perturber's orbit excite its eccentricity, we show that corotation resonances in these regions become ineffective at eccentricity damping if the object is embedded in a continuous disk without a gap. However, under these conditions another class of Lindblad resonances exists that has not been included in earlier treatments of this problem. These operate on disk material co-orbiting with the perturber and become the most important source of eccentricity damping. We employ a model problem to obtain estimates of the various disk torques and conclude, therefrom, that the eccentricity ultimately suffers decay. The limitations of this model are also discussed, as is the need for further studies.

I. INTRODUCTION

In an important paper, Goldreich and Tremaine (1980, hereafter referred to as GT80) studied the semimajor axis and eccentricity changes that are produced by the reaction torque of a disk perturbed by the gravitational field of an orbiting object. They demonstrated that a perturber, orbiting near a ring, will recoil from the ring and suffer a damping of its orbital eccentricity. Interestingly, the eccentricity damping depended on a slight (i.e., ~5%) dominance of the corotation torques over competing Lindblad torques, which work to increase e. In addition to obvious planetary ring applications, such density wave interactions may have played an important role in the early Solar System. Indeed, this was recognized by Goldreich and Tremaine (GT80), who extended their results for a finite ring to the case of a planet orbiting within a continuous disk, intended to represent the solar nebula. They argued that although the planet repels both interior and exterior portions of the disk, gradients in the disk's properties should lead to a differential torque of order $\sim h/r$ times the disk–planet torque from either side, h being the disk scale height. This results in an overall radial drift of the orbit and estimates of this rate as well as that for eccentricity damping were then made for Jupiter.

Hourigan and Ward (1984) and Ward (1986) pursued the question of radial migration further, pointing out its possible importance to the planetary accretion process. In models where accretion occurs through stochastic collisions among planetesimals (e.g., Safronov 1972, Wetherill 1980), the preponderance of accretion time occurs in the terminal stages, where objects are few and relatively remote. Under certain conditions, accretion time scales could be shortened considerably by increased radial mobility. Of course, aerodynamic drag has long been suggested as a source of orbital decay for smaller objects (Whipple 1972, Weidenschilling 1977, Adachi *et al.* 1976). However, density waves appear to provide a complementary mechanism that dominates in the large size range.

It is natural to suspect that this comple-

[1] Also Adjunct Professor, Dept. of Physics, Harvey Mudd College, Claremont, CA 91711.

0019-1035/88 $3.00

mentary behavior extends to orbital eccentricities and inclinations as well, both of which are known to be damped by aerodynamic drag (e.g., Safronov 1972, Adachi *et al.* 1976). In this context, the eccentricity damping predicted in GT80 does not seem surprising. Curiously, however, Borderies *et al.* (1984) have subsequently concluded that bending wave interactions with a ring increase the perturber's inclination, a behavior which, itself, may provide important constraints for early Solar System models. The perturber's inclination increases because vertical resonances are analogs of Lindblad resonances, while there are no corresponding analogs of corotation resonances in the vertical problem. Goldreich and Tremaine (1981) have further proposed that the observed ring eccentricities of the Uranus system may be due to a partial weakening of corotation torques through saturation effects. This suggests that the damping of eccentricities in the solar nebula bears careful reexamination with particular emphasis on verifying the strength of the corotation terms.

II. RING AND DISK TORQUES

We begin by briefly reviewing existing calculations of ring and disk torques and their effects on the eccentricity. The variation in the perturber's eccentricity due to a disk reaction torque, T_r, is given by (GT80)

$$\frac{1}{e}\frac{de}{dt} = \left[(\Omega_{ps} - \Omega_p) - 2e^2\Omega_p\left(1 + \frac{d\ln\kappa}{d\ln r}\right)_{r=a}\right]\frac{T_r}{M_p(ea\kappa)^2}. \quad (1)$$

The pattern speed Ω_{ps} associated with torque T_r is $\Omega_{ps} = \Omega_p + (l - m)\kappa_p/m$, where Ω_p and κ_p are the guiding center and epicycle frequencies of the perturber of mass M_p, and a and e denote the semimajor axis and the eccentricity. For a Keplerian disk, $\Omega^2 = \kappa^2 = GM_\odot/r^3$, $\Omega_p^2 = \kappa_p^2 = GM_\odot/a^3$, and Eq. (1) simplifies to

$$\frac{1}{e}\frac{de}{dt} = \left[\frac{l - m}{m} + e^2\right]\frac{T_r}{M_p e^2 a^2 \Omega_p}. \quad (2)$$

The disturbing potential $V = -GM_p/|\mathbf{r} - \mathbf{r}_p|$ is Fourier decomposed into the form $V = \sum_{l=-\infty}^{\infty}\sum_{m=0}^{\infty}\phi_{l,m}\cos\{m\theta - [m\Omega_p + (l - m)\kappa_p]t\}$, with $\mathbf{r}_p$ locating the perturber and θ being an azimuthal coordinate measured in the plane of the disk. The potential amplitudes $\phi_{l,m}$ are proportional to $e^{|l-m|}$. Figure 1, adapted from GT80, shows the positions, relative to the perturber's semimajor axis, of those resonances with $|l - m| \le 1$. For each potential term there is both an inner and outer Lindblad [$\kappa^2 = m^2(\Omega - \Omega_{ps})^2$] and a single corotation [$\Omega = \Omega_{ps}$] resonance. The potential amplitudes are

$$\phi_{m,m} = -\frac{GM_p}{a} b^m_{1/2}(\gamma_0) \quad (3a)$$

$$\phi_{m\pm1,m} = -e\frac{GM_p}{2a}\left[\gamma_0\frac{db^m_{1/2}}{d\gamma_0} + (1 \pm 2m)b^m_{1/2}\right], \quad (3b)$$

where $b^m_{1/2}(\gamma_0)$ are Laplace coefficients (e.g., Brouwer and Clemence 1961) and $\gamma_0 = r/a$. [Eqs. (3a) and (3b) ignore the indirect part of the disturbing function as well as direct axisymmetric terms ($m = 0$).]

The strongest Lindblad resonances are

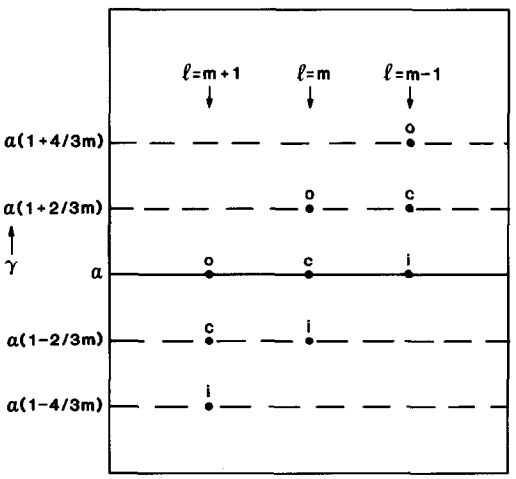

FIG. 1. Positions of $|l - m| \le 1$ resonances in a Keplerian disk relative to semimajor axis a of the perturber. The symbols o, c, and i denote outer Lindblad resonances, corotation resonances, and inner Lindblad resonances, respectively (adapted from Goldreich and Tremaine 1980).

those with $l = m$ and can significantly influence the semimajor axis (GT80, see also Ward 1986). However, they produce a contribution to $\dot{e}$ of order $O(em^2)(\mu\Omega)(\sigma a^2/M_\odot)$, where $\mu = M_p/M_\odot$ and σ is the disk's surface density. This contribution is down by a factor $(1/m)$ from $|l - m| = 1$ resonances discussed below. In addition, inner and outer $l = m$ resonances oppose each other, further weakening their importance for the eccentricity of a perturber embedded in a disk.

The strongest corotation resonances ($l = m$) fall *at* the perturber's semimajor axis, as do the outer (inner) Lindblad resonances with $l = m + 1$ ($l = m - 1$). Torques derived by standard linear techniques for a two-dimensional disk [Eqs. (4) and (9) below] are not valid expression for resonances that *coorbit* with the perturber. However, this issue can be sidestepped if the perturber lies completely outside the disk or resides in a gap where the surface density, $\sigma \to 0$. Most applications to Saturnian and Uranian ring systems fall into this category (e.g., Goldreich and Tremaine 1978, 1981, Lissauer *et al.* 1981, Shu 1984), as have calculations of protoplanet truncations of the solar nebula (Papaloizou and Lin 1984, Lin and Papaloizou 1986). We will return to this issue in Section III.

For resonances located interior or exterior to the perturber's orbit, substitution of a given potential component into the linearized equations of motion and continuity equation allows for the calculation of surface density perturbations. The attraction of the perturber for these perturbations then yields the sought-after disk torque. Such calculations are well documented in the literature and their results are summarized as follows.

Lindblad resonances. For waves launched at an mth-order Lindblad resonance the torque on the perturber reads (e.g., Lynden-Bell and Kalnajs 1972, Goldreich and Tremaine 1978, 1979)

$$T^L_{l,m} = m\pi^2\sigma\Psi^2_{l,m}/\mathcal{D}, \tag{4}$$

where $D = \kappa^2 - m^2(\Omega - \Omega_{ps})^2$, $\mathcal{D} = (r\, dD/dr)_{r_L}$, r_L being the resonance position in the disk [$D(r_L) = 0$]. The forcing term $\Psi_{l,m}$ is related to the amplitude potentials through the expression

$$\Psi_{l,m} = r\frac{d\phi_{l,m}}{dr} + \frac{2\Omega\phi_{l,m}}{\Omega - \Omega_{ps}} = r\frac{d\phi_{l,m}}{dr} - 2\varepsilon m\left(\frac{\Omega}{\kappa}\right)\phi_{l,m}, \tag{5}$$

where $\varepsilon = -\mathrm{sgn}(\mathcal{D}) = \pm 1$ for outer and inner resonances, respectively. Combining (3b) and (5) yields

$$\Psi_{m-\varepsilon,m} = -e\frac{GM_p}{2a}\left\{\gamma^2\frac{d^2b^m_{1/2}}{d\gamma^2} - 4\varepsilon m\gamma\frac{db^m_{1/2}}{d\gamma} + 4m^2b^m_{1/2}\right\} \approx -e\frac{GM_p}{a}\frac{m^2}{\pi}\left\{\frac{19}{4}K_1(4/3) + 5K_0(4/3)\right\}, \tag{6}$$

where $\Psi_{l,m}$ has been evaluated at the resonance point, $\gamma_L \cong (1 + \varepsilon/m)^{2/3}(1 - \varepsilon/m)^{-2/3} \approx 1 + \varepsilon(4/3m)$. (The use of modified Bessel functions K_i to approximate Laplace coefficients is justified in GT80.) From (2) and (4) we find the torque to the lowest order,

$$T^L_{m-\varepsilon,m} = -\varepsilon\frac{e^2\sigma}{3}\left(\frac{GM_p}{a\Omega}\right)^2 m^4\left\{\frac{19}{4}K_1(4/3) + 5K_0(4/3)\right\}^2, \tag{7}$$

and its contribution to $\dot{e}$,

$$\left(\frac{1}{e}\frac{de}{dt}\right)^L_{m-\varepsilon,m} = \frac{1}{3}m^3\mu\Omega_p\left(\frac{\sigma a^2}{M_\odot}\right)\left\{\frac{19}{4}K_1(4/3) + 5K_1(4/3)\right\}^2. \tag{8}$$

Note that *both* inner and outer resonances increase the eccentricity.

Corotation resonances. For an mth-order corotation resonance the torque is (e.g., Donner 1978, Goldreich and Tremaine 1979)

$$T^C_{l,m} = -\frac{\pi^2 m}{2}\left[\frac{\phi^2_{l,m}}{d\Omega/dr}\frac{d}{dr}\left(\frac{\sigma}{B}\right)\right]_{r_C}, \tag{9}$$

where $B = \Omega + (r/2)d\Omega/dr$ is the Oort number. For a Keplerian disk, $B = \Omega/4$. The

resonance locations are $\gamma_C = r_C/r_p = (1 - \varepsilon/m)^{-2/3} \approx 1 + \varepsilon(2/3m)$ and to lowest order in m^{-1},

$$\phi_{m-\varepsilon,m} \approx \varepsilon e m \frac{GM_p}{\pi a} [K_1(2/3) + 2K_0(2/3)]. \quad (10)$$

Combining (9) and (10) for a Keplerian disk,

$$T^C_{m-\varepsilon,m} = \frac{4}{3} e^2 m^3 \left(\frac{GM_p}{a\Omega}\right)^2 r\Omega \frac{d}{dr}\left(\frac{\sigma}{\Omega}\right) [K_1(2/3) + 2K_0(2/3)]^2. \quad (11)$$

The contribution of the corotation torque to $\dot{e}$ is

$$\left(\frac{1}{e}\frac{de}{dt}\right)^C_{m-\varepsilon,m} = -\frac{4}{3}\varepsilon m^2 \mu \frac{a^3\Omega^2}{M_\odot}\frac{d}{dr}\left(\frac{\sigma}{\Omega}\right)[K_1(2/3) + 2K_0(2/3)]^2, \quad (12)$$

to lowest order in e and m^{-1}. Note that Eq. (12) has an explicit ε dependence, while (8) does not.

Goldreich and Tremaine determine the total eccentricity variation of a satellite due to interaction with a ringlet of width δr, mass $M_r = 2\pi\sigma r\delta r$, lying a distance Δr inside or outside the perturber's orbit by summing contributions (8) and (12) over the appropriate range of resonances, δm. For Lindblad resonances with $m^L \sim (4/3)(a/\Delta r)$, $\delta m^L \sim (4/3)(a/\Delta r)(\delta r/\Delta r)$,

$$\left(\frac{1}{e}\frac{de}{dt}\right)^L_{\text{ring}} \approx \delta m \left(\frac{1}{e}\frac{de}{dt}\right)^L_{m-\varepsilon,m} \approx \frac{2^7}{\pi 3^5}\mu\Omega\left(\frac{M_r}{M_\odot}\right)\left|\frac{a}{\Delta r}\right|^5\left\{\frac{19}{4}K_1(4/3) + 5K_0(4/3)\right\}^2, \quad (13a)$$

while for corotation resonances, $m^C \sim (2/3)(a/\Delta r)$, $\delta m^C \sim (2/3)(a/\Delta r)(\delta r/\Delta r)$, and

$$\left(\frac{1}{e}\frac{de}{dt}\right)^L_{\text{ring}} = \int_{\text{ring}} dm \left(\frac{1}{e}\frac{de}{dt}\right)^C_{m-\varepsilon,m} \approx -\frac{2^6}{\pi 3^4}\mu\Omega\left(\frac{M_r}{M_\odot}\right)\left|\frac{a}{\Delta r}\right|^5 [K_1(2/3) + 2K_0(2/3)]^2. \quad (13b)$$

Integration in (13b) is necessary even for a very narrow ring because corotation torques are proportional to the gradient of the surface density per unit vorticity and this quantity varies considerably across an isolated ringlet with real edges. The ratio $|de/dt|^L/|de/dt|^C \approx 0.954$ and

$$\left(\frac{1}{e}\frac{de}{dt}\right)^L + \left(\frac{1}{e}\frac{de}{dt}\right)^C \approx -0.073\mu\Omega\left(\frac{M_r}{M_\odot}\right)\left|\frac{a}{\Delta r}\right|^5, \quad (14)$$

i.e., the damping effect of corotation resonances dominates by about 5%. Equation (14) is valid for rings lying at a distance from the perturber greater than the scale height of the ring.

Extension of these results to a wide disk of material is straightforward if the disk is considered to be a collection of ringlets and the torques (4) and (9) remain valid. This latter condition requires $c \ll r\Omega$ and $m \ll r\kappa/c$, where c is the disperson velocity. Ringlets closer to the planet than $\Delta r \sim O(r/m) \leq O(c/\kappa)$ will thus violate the second criterion and lie within what is termed by GT80 as the region of torque cutoff. The divergence of torque strength as $m \to \infty$ predicted by Eqs. (7) and (11) does not apply in this zone. Lindblad resonances with $\xi = mc/r\kappa \gg 1$ weaken because disk pressure displaces the launch point away from the perturber where the forcing function is weaker. Although the locations of corotation resonances are relatively unaffected, disk pressure still works to suppress the amplitude and radial extent of the disk's response. Such resonances may also suffer significant saturation. In addition, corrections for finite disk thickness should become increasingly important for resonances that lie near the perturber. We denote the ratio of actual torque to either (7) or (11) as the torque cutoff function, $f_{\text{res}}(\xi)$. This ratio was numerically calculated for $l = m$ Lindblad resonances in a $Q = \infty$ disk in GT80. If we follow GT80 and assume a similar behavior for $|l - m| = 1$ resonances, (8)

is easily extended to a continuous disk by integrating over all orders,

$$\left(\frac{1}{e}\frac{de}{dt}\right)^{\mathrm{L}}_{\mathrm{disc}} = \frac{\xi^4_{\mathrm{L},4}}{6}\,\mu\Omega\left(\frac{\sigma a^2}{M_\odot}\right)\left(\frac{a\Omega}{c}\right)^4\left\{\frac{19}{4}\,K_1(4/3) + 5K_0(4/3)\right\}^2, \quad (15)$$

where the torque cutoff parameter, ξ_n, is defined by

$$\frac{1}{n}\,(\xi_n)^n = \int_0^\infty \xi^{n-1} f(\xi)\,d\xi. \quad (16)$$

For the problem at hand, $\xi_{\mathrm{L},4} = 0.85$ (Ward 1986). Equation (15) includes contributions from resonances both interior and exterior to the orbit. Acting alone, these excite the perturber's eccentricity on a characteristic time scale,

$$\tau = e/\dot{e} \sim 1.3\mu^{-1}\Omega^{-1}(M_\odot/\sigma a^2)(c/a\Omega)^4. \quad (17)$$

Equation (17) can be used to illustrate the importance of our problem for the early Solar System. The following values will be adopted as appropriate for a minimum mass model of the solar nebula: $M_\odot = 2 \times 10^{33}$ g, $a = 1.5 \times 10^{15}\,a'$ cm, $T = T_2 \times 10^2$ °K, $\sigma = \sigma_2 \times 10^2$ g/cm^2, $c = 7.6 \times 10^3\,T^{1/2}$ cm/sec, and $\Omega = 2 \times 10^{-7}\,a'^{-3/2}$ sec. For an Earth-sized object ($\mu_\oplus = 3 \times 10^{-6}$) in the terrestrial zone with $\sigma_2 \sim 10$, $T_2 \sim 10$, $a' \sim 1$; $\tau \sim 2.5 \times 10^4$ years. This time is some two to three orders of magnitude shorter than typical time scales quoted for the stochastic accretion of such an object (e.g., Safronov 1972, Wetherill 1980). Equation (17) is also short compared to eccentricity damping by aerodynamic drag (e.g., Nakano 1987), $\tau_{\mathrm{drag}} \sim (4/\pi C_D)e^{-1}\mu^{-1}\Omega^{-1}(M_\odot/\sigma r^2)(c/r\Omega)^5$. Comparison of these time scales reveals $\tau_{\mathrm{drag}}/\tau_{\mathrm{L}} \sim O[e^{-1}(c/r\Omega)] \gg 1$ as long as the relative motion is subsonic, $er\Omega \ll c$.

Including corotation resonances is slightly more subtle. One cannot simply extend Eq. (14) by multiplying it with a single cutoff function and integrating over m [although such a procedure reproduces the expression (Eq. 110, GT80) used to estimate the eccentricity damping time for Jupiter]. First, Lindblad, f_{L}, and corotation, f_{C}, cutoff functions may not be identical. Second, Lindblad resonances are roughly twice the order (i.e., $m_{\mathrm{L}} = 2m_{\mathrm{C}}$) of corotation resonances at any given distance from the perturber. Finally, Eq. (13b) already contains an integration and the torque cutoff function, $f_{\mathrm{C}}(\xi)$, must be included *inside* its integrand. The sensitive nature of differencing two nearly equal rates makes it apparent that for objects orbiting within a scale height of the disk's edge, reliable estimates of their eccentricity variation will require explicit determinations of the relevant torque cutoff functions, a task that is under development now. However, for objects completely embedded in a continuous disk there is a more straightforward reason to question the damping power of corotation torques—one that is not overly sensitive to the cutoff functions.

Inspection of Eqs. (8) and (12) reveals that while Lindblad torques always excite e, corotation torques may either excite or damp the eccentricity, depending (i) on whether they fall exterior or interior to the orbit ($\varepsilon = \pm 1$) and (ii) on the sign of the gradient. If the perturber orbits near a free edge, the gradient is dominated by changes in the surface density so that $\mathrm{sgn}[d(\sigma/B)/dr] = \varepsilon$. This explains why the eccentricity is damped by corotation torques for a perturber lying either completely outside a disk or in a gap. However, if the perturber is embedded in a disk whose gradient $d(\sigma/B)/dr$ changes little across the orbit, exterior and interior corotation resonances largely compensate each other and $(\dot{e}/e)^{\mathrm{C}}$ must come from differential effects, i.e.,

$$\left(\frac{1}{e}\frac{de}{dt}\right)^{\mathrm{C}}_{\mathrm{disc}} \sim -\frac{8}{9}\,\xi^2_{\mathrm{C},2}\,\mu\Omega\left[\frac{a^4\Omega}{M_\odot}\frac{d^2}{dr^2}\left(\frac{\sigma}{\Omega}\right)\right]\left(\frac{a\Omega}{c}\right)^2[K_1(2/3) + 2K_0(2/3)]^2. \quad (18)$$

In deriving (18), $d(\sigma/\Omega)/dr$ has been expanded to the lowest order about its value at the perturber's orbit. Note that $(\dot{e}/e)^C < 0$ only if $d^2(\sigma/\Omega)/dr^2 < 0$ and that Eq. (18) is smaller than Eq. (15) if $d^2(\sigma/\Omega)/dr^2 \ll (\sigma/\Omega)/h^2$.

This argument suggests that planetesimals that are too small to open a gap in the solar nebula will not experience significant eccentricity damping through corotation torques. The critical size necessary to open and maintain a gap in the nebula has been discussed elsewhere (e.g., Lin and Papaloizou 1979, 1986, Papaloizou and Lin 1984, Hourigan and Ward, 1984, Ward 1986) but for typical solar nebular models can be of planetary scale, $\mu \gtrsim O(10^{-6})$. However, we must remember that this argument against corotation torques now makes it impossible to sidestep the issue of co-orbital resonances, since a continuous disk implies that disk material occupies the perturber's orbit. Unfortunately, the linearized techniques used to such advantage in previous analyses cannot be employed so easily for co-orbital resonances.

III. CO-ORBITAL TORQUES

A principal difficulty in treating co-orbital resonances is the divergence of the potential amplitudes [(3a) and (3b)] as $r \to a$, $\gamma_0 \to 1$. This is a characteristic of Laplace coefficients used in expanding the (direct) disturbing function,

$$V = -\frac{GM_p}{|\mathbf{r} - \mathbf{r}_p|} = -\frac{GM_p}{r_p}\left\{\frac{1}{2} b^0_{1/2}(\gamma) + \sum b^m_{1/2}(\gamma) \cos m(\theta - \theta_p)\right\}, \quad (19a)$$

where $\gamma = r/r_p$ and

$$b^m_{1/2}(\gamma) = \frac{2}{\pi}\int_0^\pi \frac{\cos m\lambda \, d\lambda}{\sqrt{1 - 2\gamma \cos \lambda + \gamma^2}}, \quad (19b)$$

and is physically artificial because it assumes that the perturbing object is a point mass. This problem can be largely circumvented by considering the finite thickness of the disk, $h \sim c/\Omega$. We replace $\mathbf{r} \to \mathbf{r} + z\mathbf{k}$, where z measures height above the midplane. This leads to a replacement of standard coefficients with a generalized form

$$b^m_{1/2}(\gamma, z) = \frac{2}{\pi}\int_0^\pi \frac{\cos m\lambda \, d\lambda}{\sqrt{1 - 2\gamma \cos \lambda + \gamma^2 + (z/r_p)^2}}, \quad (20a)$$

which can, as before, be approximated by modified Bessel functions,

$$b^m_{1/2}(\gamma, z) \approx \frac{2}{\pi} K_0(\sqrt{m^2(1 - \gamma)^2 + (mz/r_p)^2}), \quad (20b)]$$

if $m \gg 1$, $(1 - \gamma)^2 + (z/r_p)^2 \ll 1$. Divergence at $\gamma = 1$ is now avoided except when $z \equiv 0$, reflecting the fact that even at the "same orbital radius," disk material is generally a finite distance (i.e., in the z-direction) from the perturber. However, V varies considerably with height and the problem is now a strictly three-dimensional one, especially for portions of the disk within a scale height of the perturber. We can nevertheless define a useful auxiliary problem that can be solved by a minor modification of existing techniques.

We adopt a density profile $\rho = (\sigma/h)\pi^{-1/2} \exp[-(z/h)^2]$, appropriate for an unperturbed isothermal disk, and vertically average the disturbing function,

$$\langle V \rangle = -\frac{GM_p}{r_p}\left\{\frac{1}{2}\langle b^0_{1/2}\rangle + \sum \langle b^m_{1/2}\rangle \cos m(\theta - \theta_p)\right\}, \quad (21)$$

where

$$\langle b^m_{1/2}\rangle \approx \frac{2}{\pi}\langle K_0\rangle = \frac{2}{\pi^{3/2}h}\int_{-\infty}^{\infty} e^{-(z/h)^2} K_0(\sqrt{m^2(1 - \gamma)^2 + (mz/r_p)^2})\, dz = \frac{2}{\pi^{3/2}\xi}\int_{-\infty}^{\infty} e^{-(t/\xi)^2} K_0(\sqrt{m^2(1 - \gamma)^2 + t^2})\, dt. \quad (22)$$

Figure 2 displays the behavior of $\langle b^m_{1/2}\rangle$ as a function of $\alpha = m|1 - \gamma|$ for various ξ. We shall then calculate the response of a two-dimensional disk to such a potential. Admittedly, this procedure is too crude to furnish precise values for the co-orbital torques, nevertheless it should provide valuable insight as to their sign and order of magnitude.

Our strategy will be to compare a given mth-order co-orbital resonance with its mth-order interior or exterior counterpart. In order to make such a comparison consistently, we must apply the same vertical averaging techniques to all torques. This can be done for exterior and interior torques by replacing Laplace coefficients and their derivatives in Eqs. (6) and (9) with their average values. For $\xi \gg 1$, the exponential term in Eq. (22) can be ignored and the result integrated to give

$$\langle b^m_{1/2}\rangle = \frac{2}{\sqrt{\pi}}\,\xi^{-1}e^{-\alpha};$$

$$\frac{d^n}{d\gamma^n}\langle b^m_{1/2}\rangle = \frac{2}{\sqrt{\pi}}\,\xi^{-1}m^n e^{-\alpha}\,\mathrm{sgn}^n(1-\gamma). \tag{23}$$

In this case, forcing amplitudes are easily found,

$$\langle \phi_{m-\varepsilon,m}\rangle = 3\varepsilon e\,\frac{GM_p}{h\sqrt{\pi}}\,e^{-\alpha};$$

$$\langle \Psi_{m-\varepsilon,m}\rangle = -9me\,\frac{GM_p}{h\sqrt{\pi}}\,e^{-\alpha}. \tag{24}$$

Note that averaging drops their power dependence on m by 1 and consequently that of their corresponding torques by m^2. In general we set

$$\langle b^m_{1/2}\rangle = \frac{2}{\sqrt{\pi}}\,\xi^{-1}\mathcal{F}_0(\alpha,\xi)$$

$$\frac{d}{d\gamma}\langle b^m_{1/2}\rangle = \mathrm{sgn}(1-\gamma)\,\frac{2m}{\sqrt{\pi}}\,\xi^{-1}\mathcal{F}_1(\alpha,\xi)$$

$$\frac{d^2}{d\gamma^2}\langle b^m_{1/2}\rangle = \frac{2m^2}{\sqrt{\pi}}\,\xi^{-1}\mathcal{F}_2(\alpha,\xi), \tag{25}$$

where $\mathcal{F}_n = (-1)^n d^n\mathcal{F}_0/d\alpha^n$, i.e.,

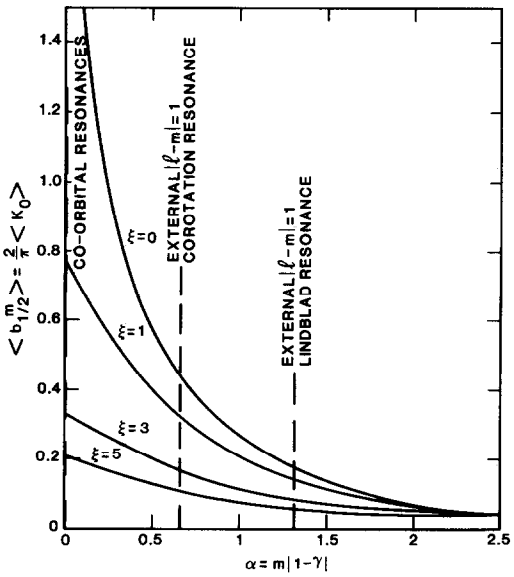

FIG. 2. Averaged Laplace coefficient, $\langle b^m_{1/2}\rangle$, as a function of $\alpha = m|1 - \gamma|$ for various values of ξ. Also shown are locations of Lindblad and corotation resonances.

$$\mathcal{F}_0(\alpha,\xi) = \pi^{-1}\int_{-\infty}^{\infty} e^{-(t/\xi)^2}K_0\left(\sqrt{\alpha^2+t^2}\right)dt$$

$$\mathcal{F}_1(\alpha,\xi) = \pi^{-1}\int_{-\infty}^{\infty} e^{-(t/\xi)^2}\frac{\alpha K_1\left(\sqrt{\alpha^2+t^2}\right)}{\sqrt{\alpha^2+t^2}}\,dt$$

$$\mathcal{F}_2(\alpha,\xi) = \pi^{-1}\int_{-\infty}^{\infty} e^{-(t/\xi)^2}\left\{\frac{K_1\left(\sqrt{\alpha^2+t^2}\right)}{\sqrt{\alpha^2+t^2}} - \frac{\alpha^2 K_2\left(\sqrt{\alpha^2+t^2}\right)}{\alpha^2+t^2}\right\}dt. \tag{26}$$

Then for Lindblad resonances ($\alpha = 4/3$),

$$\langle \Psi_{m-\varepsilon,m}\rangle = -e\,\frac{GM_p}{a}\,\frac{m}{\sqrt{\pi}}\left(\frac{a\Omega}{c}\right)\{\mathcal{F}_2(4/3,\xi) + 4\mathcal{F}_1(4/3,\xi) + 4\mathcal{F}_0(4/3,\xi)\}, \tag{27}$$

while for corotation resonances ($\alpha = 2/3$),

$$\langle \phi_{m-\varepsilon,m}\rangle = \varepsilon e\,\frac{GM_p}{a}\,\frac{1}{\sqrt{\pi}}\left(\frac{a\Omega}{c}\right)\{\mathcal{F}_1(2/3,\xi) + 2\mathcal{F}_0(2/3,\xi)\}. \tag{28}$$

Needed values for $\mathcal{F}_n(4/3,\xi)$ are determined by numerical integration and shown in Fig. 3. The averaged torques are found by substituting (27) and (28) into (4) and (9).

Corresponding eccentricity variations are

$$\left(\frac{1}{e}\frac{de}{dt}\right)^{L} = \frac{\pi}{3} m \left(\frac{a\Omega}{c}\right)^2 \mu\Omega \left(\frac{\sigma a^2}{M_\odot}\right) \{\mathcal{F}_2 + 4\mathcal{F}_1 + 4\mathcal{F}_0\}^2_{\alpha=4/3} \quad (29)$$

$$\left(\frac{1}{e}\frac{de}{dt}\right)^{C} = -\varepsilon \frac{4\pi}{3} \left(\frac{a\Omega}{c}\right)^2 \mu \left(\frac{a^3\Omega^2}{M_\odot}\right)\left(\frac{d}{dr}\frac{\sigma}{\Omega}\right) \{\mathcal{F}_1 + 2\mathcal{F}_0\}^2_{\alpha=2/3}. \quad (30)$$

These rates are now "adjusted" for the torque dilution of the disk's finite thickness. [We should emphasize that this is distinct and separate from the torque cutoff phenomenon mentioned in Section II and which should still be applied in some form to (29) and (30).]

We now perform the complimentary procedure for co-orbital resonances. However, the situation is complicated by an annulus of disk material between the perturber's perihelion and aphelion which must experience sign reversals in the radial force each orbit. Hence, care must be taken that this trait is properly accounted for when forcing terms are Fourier decomposed.

The averaged Laplace coefficient is first expanded about $\gamma = 1$,

$$\langle b^m_{1/2}(\gamma)\rangle \approx \langle b^m_{1/2}\rangle_{\gamma=1} - \left.\frac{\partial\langle b^m_{1/2}\rangle}{\partial\gamma}\right|_{\gamma=1} (1-\gamma) + \frac{1}{2}\left.\frac{\partial^2\langle b^m_{1/2}\rangle}{\partial\gamma^2}\right|_{\gamma=1} (1-\gamma)^2 + \cdots \quad (31)$$

The lead term is a well-known Bessel function integral (e.g., Abramowitz and Stegun 1964)

$$\langle b^m_{1/2}\rangle_{\gamma=1} = \frac{2}{\pi^{3/2}\xi}\int_{-\infty}^{\infty} e^{-(t/\xi)^2} K_0(|t|)\, dt = \pi^{-1} e^{\xi^2/8} K_0(\xi^2/8). \quad (32)$$

Following through with previous notation we write $\langle b^m_{1/2}\rangle_{\gamma=1} = (2/\sqrt{\pi})\xi^{-1}\mathcal{F}_0(0, \xi)$, where

$$\mathcal{F}_0(0, \xi) = \lim_{\alpha\to 0} \mathcal{F}_0(\alpha, \xi) = \frac{\xi}{2\sqrt{\pi}} e^{\xi^2/8} K_0(\xi^2/8). \quad (33)$$

Similarly, the first derivative can be written

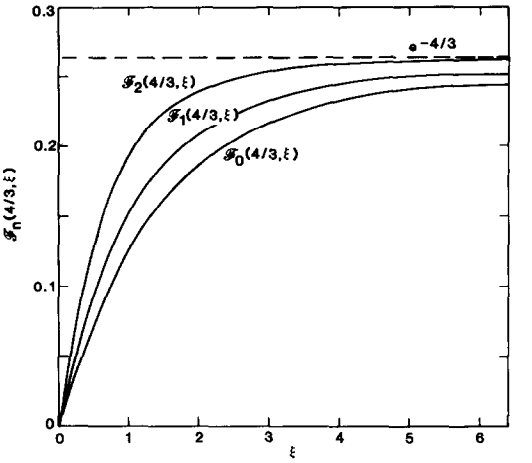

FIG. 3. Amplitude components $\mathcal{F}_n(4/3, \xi)$ vs ξ for vertically averaged exterior and interior Lindblad resonances.

$$\left.\frac{\partial\langle b^m_{1/2}\rangle}{\partial\gamma}\right|_{\gamma=1} = \mathrm{sgn}(1-\gamma)\frac{2m}{\pi^{3/2}\xi}\lim_{\alpha\to\infty} \int_{-\infty}^{\infty} e^{-(t/\xi)^2}\frac{\alpha K_1(\sqrt{\alpha^2+t^2})}{\sqrt{\alpha^2+t^2}}\, dt = \mathrm{sgn}(1-\gamma)\frac{2m}{\sqrt{\pi}}\xi^{-1}\mathcal{F}_1(0, \xi). \quad (34)$$

As $\alpha \to 0$, $K_1(\sqrt{\alpha^2+t^2}) \to (\alpha^2+t^2)^{-1/2}$ and $\alpha K_1/(\alpha^2+t^2)^{1/2} \to \alpha/(\alpha^2+t^2) \to \pi\delta(t)$, where $\delta(t)$ denotes the Dirac delta function. Hence, $\mathcal{F}_1(0, \xi) \equiv 1$. Finally, the second derivative can be written

$$\frac{\partial^2\langle b^m_{1/2}\rangle}{\partial\gamma^2} = -\frac{2m^2}{\pi^{3/2}\xi}\lim_{\alpha\to 0}\int_{-\infty}^{\infty} e^{-(t/\xi)^2}\left\{\frac{K_1(\sqrt{\alpha^2+t^2})}{\sqrt{\alpha^2+t^2}} - \alpha^2\frac{K_2(\sqrt{\alpha^2+t^2})}{\alpha^2+t^2}\right\} dt = \frac{2m^2}{\sqrt{\pi}\xi}\mathcal{F}_2(0, \xi). \quad (35)$$

The function $\mathcal{F}_2(0, \xi)$ can be approximated analytically for both high and low values of ξ. If $\xi \gg 1$, the exponential term can be ignored with little error. Changing the integration variable to $x = 1 + (t/\alpha)^2$ and using the definite integral $\int_1^\infty x^{-\nu/2}(x-1)^{\mu-1}K_\nu(\alpha\sqrt{x})\, dx = \Gamma(\mu)(2/\alpha)^\mu K_{\nu-\mu}(\alpha)$ (e.g., Gradshteyn and Ryzhik 1965), one obtains,

$$\mathcal{F}_2(0, \xi) = \lim_{\alpha \to 0} \left(\frac{2}{\alpha}\right)^{1/2} \frac{\Gamma(1/2)}{\pi} [\alpha K_{3/2}(\alpha) - K_{1/2}(\alpha)] = 1 \quad (36)$$

[This result is also found from $\mathcal{F}_2 = d^2\mathcal{F}_0/d\alpha^2$ together with (23) in the limit $\alpha \to 0$.] For $\xi \ll 1$, the exponential kills the integrand while Bessel function arguments are small and $K_\nu(z) \approx (1/2)\Gamma(\nu)(z/2)^{-\nu}$ is a good approximation. In this case,

$$\mathcal{F}_2(0, \xi) \approx -\pi^{-1} \lim_{\alpha \to 0} \frac{d}{d\alpha} \int_{-\infty}^{\infty} e^{-(t/\xi)^2} \frac{\alpha\, dt}{\alpha^2 + t^2} = -\pi^{-1} \lim_{\alpha \to 0} \frac{d}{d\alpha} \pi e^{(\alpha/\xi)^2} \operatorname{erfc}(\alpha/\xi) = \frac{2}{\sqrt{\pi}} \xi^{-1}. \quad (37)$$

The complete function $\mathcal{F}_2(0, \xi)$ can be found by numerical integration and is shown in Fig. 4 along with $\mathcal{F}_0(0, \xi)$.

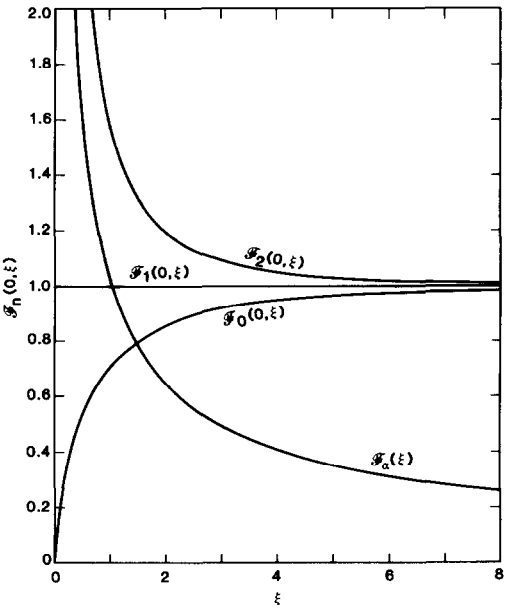

FIG. 4. Amplitude components $\mathcal{F}_n(0, \xi)$ vs ξ for vertically averaged co-orbital Lindblad resonances.

Substitution of (32), (34), and (35) into (31) yields

$$\langle b^m_{1/2} \rangle \approx \frac{2}{\sqrt{\pi}} \xi^{-1} \left[\mathcal{F}_0(0, \xi) - m|1 - \gamma| + \frac{1}{2} m^2 \mathcal{F}_2(0, \xi)(1 - \gamma)^2 + \cdots\right]. \quad (38)$$

If the perturber has an eccentric orbit, terms containing $1 - \gamma$ are periodic in the epicycle frequency, κ_p. To the lowest order in e,

$$1 - \gamma \approx 1 - \gamma_0 - e\gamma_0 \cos f, \quad (39)$$

where $\gamma_0 = r/a$ and $f = \kappa_p t$. The Laplace coefficients can be expressed as a Fourier series in terms of κ_p and its harmonics,

$$-\frac{GM_p}{r_p} \langle b^m_{1/2} \rangle = \frac{1}{2} A_0 + \sum_{k=1}^{\infty} A_k \cos kf. \quad (40)$$

Coefficients $\{A_k\}$ are determined in Appendix A. In addition, cosine terms in Eq. (21) must be expanded to first order in e,

$$\cos m(\theta - \theta_p) \approx \cos m(\theta - \Omega_p t) + 2em(\Omega_p/\kappa_p) \sin f \sin m(\theta - \Omega_p t). \quad (41)$$

An mth-order term in Eq. (21) becomes

$$\begin{aligned} V_m = -\frac{GM_p}{r_p} \langle b^m_{1/2} \rangle \cos m(\theta - \theta_p) &\approx \frac{1}{2} A_0 \cos m(\theta - \Omega_p t) \\ &+ \frac{1}{2} A_0 em \frac{\Omega_p}{\kappa_p} \{\cos(m\theta - [m\Omega_p + \kappa_p]t) - \cos(m\theta - [m\Omega_p - \kappa_p]t)\} \\ &+ \frac{1}{2} \sum_{k=1}^{\infty} A_k \{\cos(m\theta - [m\Omega_p + k\kappa_p]t) + \cos(m\theta - [m\Omega_p - k\kappa_p]t)\} \\ &+ \frac{1}{2} em \frac{\Omega_p}{\kappa_p} \sum_{k-1}^{\infty} A_k \{\cos(m\theta - [m\Omega_p + (k+1)\kappa_p]t) + \cos(m\theta - [m\Omega_p - (k-1)\kappa_p]t) \\ &- \{\cos(m\theta - [m\Omega_p + (k-1)\kappa_p]t) - \cos(m\theta - [m\Omega_p - (k+1)\kappa_p]t)\}. \end{aligned} \quad (42)$$

We concentrate on those components that exhibit co-orbital resonances; for each m there is a corotation term, $\langle \phi_{m,m} \rangle \cos m(\theta - \Omega_p t)$, and two Lindblad terms $\langle \phi_{m\pm1,m} \rangle$

$\cos(m\theta - [m\Omega_p \pm \kappa_p]t)$. Their amplitudes are

$$\langle \phi_{m,m} \rangle = \frac{1}{2} A_0 \tag{43}$$

$$\langle \phi_{m\pm1,m} \rangle = \pm \frac{1}{2} em \frac{\Omega_p}{\kappa_p} A_0 + \frac{1}{2} A_1 \mp em \frac{\Omega_p}{\kappa_p} A_2. \tag{44}$$

Lindblad resonances. The response of the disk to a Lindblad term is determined by substituting the appropriate $\langle \phi \rangle$ and its derivatives into the equation describing radial variations in the surface density,

$$\frac{d^2\eta}{dx^2} - \frac{1}{x}\frac{d\eta}{dx} + \beta x \eta = -r^2 \frac{d^2\langle\phi\rangle}{dr^2} + \frac{1}{x}\left[r \frac{d\langle\phi\rangle}{dr} + \frac{2\Omega\langle\phi\rangle}{\Omega - \Omega_{ps}} \right] + m^2\langle\phi\rangle, \tag{45}$$

where, for the enthalpy perturbation, $\eta = c^2\sigma'/\sigma$, σ' is the surface density perturbation, $\beta = -\mathcal{D}r^2/c^2$, and $x = \gamma_0 - 1$ measures the distance from the co-orbital point, $r = a$. The derivation of (45) and the conditions for its validity are described by Goldreich and Tremaine (1979). For the terms on the right we are to use (44) and its derivatives. Equivalently, one can first differentiate Eq. (38) with respect to r and then Fourier decompose the results, i.e.,

$$\frac{d}{dr}\langle b^m_{1/2} \rangle = \frac{2}{\sqrt{\pi}} \frac{1}{h} [\mathrm{sgn}(1-\gamma) - m\mathcal{F}_2(0,\xi)(1-\gamma) + \cdots] = \frac{1}{2} B_0 + \sum_{k=1}^{\infty} B_k \cos kf \tag{46}$$

$$\frac{d^2}{dr^2}\langle b^m_{1/2} \rangle = -\frac{2}{\sqrt{\pi}} \frac{1}{hr_p} [2\delta(1-\gamma) - m\mathcal{F}_2(0,\xi) + \cdots] = \frac{1}{2} C_0 + \sum_{k=1}^{\infty} C_k \cos kf. \tag{47}$$

We have chosen to follow this method as it allows for better tracking of the effects of the central annulus. [The first term in (47) is obtained by writing $\mathrm{sgn}(1-\gamma) = 2H(1-\gamma) - 1$, where $H(x)$ is the Heaviside step function, and then using the relationship $\delta(x) = dH(x)/dx$.] Coefficients $\{B_k\}$, $\{C_k\}$ are also determined in Appendix A. Values for $d\langle\phi\rangle/dr$ and $d^2\langle\phi\rangle/dr^2$ are found from expressions identical to (44) in form but with A_k replaced by B_k and C_k, respectively. The results to lowest order in e and $1 - \gamma_0$ are

$$\langle \phi_{m\pm1,m} \rangle = -e \frac{GM_p}{h\sqrt{\pi}} \left\{ \pm 2\mathcal{F}_2(0,\xi) + 1 - \frac{2f_c}{\pi} + \frac{1}{\pi} \sin 2f_c \right\} \tag{48}$$

$$r\frac{d}{dr}\langle \phi_{m\pm1,m} \rangle = -e \frac{GM_p}{h\sqrt{\pi}} m \left\{ \mathcal{F}_2(0,\xi) \pm 2\left[1 - \frac{2f_c}{\pi} + \frac{1}{\pi} \sin 2f_c \right] \right\} + \frac{4GM_p}{h\pi\sqrt{\pi}} \sin f_c \tag{49}$$

$$r^2 \frac{d^2}{dr^2}\langle \phi_{m\pm1,m} \rangle = \frac{GM_p}{h\sqrt{\pi}} \left\{ \frac{4}{\pi} \frac{\cot f_c}{e} \right\}. \tag{50}$$

Terms containing f_c arise only when r lies between aphelion and perihelion so that $1 - \gamma$ undergoes sign reversals. These occur when $-x = 1 - \gamma_0 = e\gamma_0 \cos f_c$. Inside of perihelion we set $f_c = 0$, while outside of aphelion, $f_c = \pi$ in (48) and (49). Equation (50) applies only for $|1 - \gamma_0| < e\gamma_0$.

The bracketed term on the right-hand side of (45) resembles (5) except that our choice of ε vs l must be reversed, i.e.,

$$\langle \Psi_{m+\varepsilon,m} \rangle = r\frac{d}{dr}\langle \phi_{m+\varepsilon,m} \rangle - 2\varepsilon m \left(\frac{\Omega}{\kappa} \right) \langle \phi_{m+\varepsilon,m} \rangle. \tag{51}$$

Unlike distant resonances, however, neither term in Eq. (51) is constant but jumps by increments of $\sim 4\varepsilon emGM_p/h\sqrt{\pi}$ across the co-orbital point (Fig. 5). Their difference, however, does remain the same on either side,

$$\langle \Psi_{m+\varepsilon,m} \rangle = \Psi_d + \Psi_a = -e \frac{GM_p m}{a\sqrt{\pi}} \left(\frac{a\Omega}{c} \right) [\mathcal{F}_2(0,\xi) - 4\mathcal{F}_0(0,\xi)] + \frac{4}{\pi} \frac{GM_p}{h\sqrt{\pi}} \sin f_c. \tag{52}$$

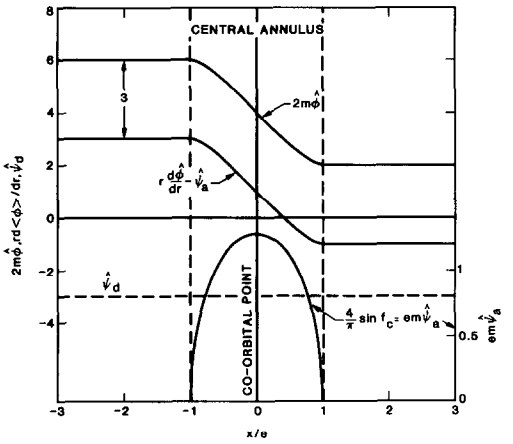

FIG. 5. Forcing functions for co-orbital Lindblad resonances used to compute radial variations in the enthalpy, η. Quantities are normalized to $-e(GM_p m/\alpha\sqrt{\pi})(a\Omega/c)$. Case shown is for $\xi \gg 1$.

Again, the last portion, Ψ_a, applies only for $|x| < e\gamma_0$. Comparison with Eq. (27) reveals another consequence of the reversed sign signature of (51). The $4\mathcal{F}_1$ term in (27) comes in equal parts from each component of (5). The analogous quantity has canceled out in Ψ_d and the remaining terms oppose each other. Finally, the forcing function also contains the non-negligible contribution [Eq. (50)] from $d^2\langle\phi\rangle/dr^2$ for $|x| < e\gamma_0$, which can be rewritten as $d\Psi_a/dx$. Introducing a new dependent variable through the defining relationship $\zeta = d\eta/dx$, the complete equation for the enthalpy variation can be written

$$\frac{d}{dx}\left[\frac{1}{x}\frac{d^2\zeta}{dx^2} + \beta\zeta\right] = -\frac{d}{dx}(\Psi_d + \Psi_a)x^{-1}, \tag{53}$$

where we can think of Ψ_d as forcing from the "whole" disk, while Ψ_a denotes forcing originating only from the central annulus. Integration of (53) yields a nonhomogeneous Airy's equation in ζ. We shall break $\eta = \eta_d + \eta_a$ into two parts and consider each in turn.

Since to our level of approximation Ψ_d is constant, the solution for η_d can be obtained by the precedure outlined by Ward (1986) and is

$$\zeta_d = \frac{\pi\Psi_d}{|\beta|^{2/3}}\{i\,\mathrm{sgn}(\beta)Ai(z) + Bi(z) - Hi(z)\} \tag{54a}$$

$$\eta_d = -\frac{\pi\Psi_d}{|\beta|^{1/3}}\left\{i\frac{dAi}{dz} + \mathrm{sgn}(\beta)\frac{dBi}{dz} - \mathrm{sgn}(\beta)\frac{dHi}{dz}\right\}, \tag{54b}$$

where $Ai(z)$, $Bi(z)$ are Airy functions, $Hi(z) = \pi^{-1}\int_0^\infty \exp[-(1/3)t^3 + zt]dt$, and $z = -\mathrm{sgn}(\beta)|\beta|^{1/3}x$. Equation (54b) is oscillatory for $z < 0$ and asymptotically becomes a trailing spiral wave,

$$\eta_d = i\sqrt{\pi}\,\Psi_d\left|\frac{x}{\beta}\right|^{1/4}\exp\left[i\,\mathrm{sgn}(\beta)\left(\frac{2}{3}|\beta x^3|^{1/2} + \frac{\pi}{4}\right)\right], \quad -z \gg 1. \tag{55}$$

For a Keplerian disk, $\mathcal{D} = -3m(\varepsilon + 1/m)\Omega^2$ and for $m > 1$, $z < 0$ implies $\mathrm{sgn}(x) = \mathrm{sgn}(\beta) = -\mathrm{sgn}(\mathcal{D}) = \varepsilon$. Since the co-orbital resonance associated with $\phi_{m\pm1}$ is an outer (inner) one, $\varepsilon = \pm 1$ and density waves propagate outward (inward) through the disk, i.e., away from the position of the associated corotation resonance. The wave train carries angular momentum by advection. The angular momentum flux at $-z \gg 1$ is (e.g., Lynden-Bell and Kalnajs 1972)

$$F_A \approx \frac{\pi m r\sigma}{D}\left[\eta_I\frac{d\eta_R}{dr} - \eta_R\frac{d\eta_I}{dr}\right], \tag{56}$$

where η is written in terms of its real and imaginary parts, $\eta = \eta_R + i\eta_I$. In the absence of other disturbance, the flux carried by (56) would be $F_A \approx m\pi^2\sigma\Psi_d^2/|\mathcal{D}|$ and the corresponding torque on the perturber is given by $T = \mathrm{sgn}(\mathcal{D})F_A$. This is just Eq. (4) with $\Psi_{l,m} \to \Psi_d$.

To solve for the disturbance generated by Ψ_a, we write

$$\zeta_a = \frac{\pi}{|\beta|^{2/3}}\left\{Ai(z)\left[i\,\mathrm{sgn}(\beta)\int_{-\infty}^{\infty}\Psi_a Ai\,dz + \int_{-\infty}^{z}\Psi_a Bi\,dz\right] + Bi(z)\int_z^\infty \Psi_a Ai\,dz\right\} \tag{57a}$$

$$\eta_a = -\frac{\pi}{|\beta|^{1/3}}\left\{\frac{d\,Ai}{dz}\left[i\int_{-\infty}^{\infty}\Psi_a Ai\,dz + \mathrm{sgn}(\beta)\int_{-\infty}^{z}\Psi_a Bi\,dz\right] + \mathrm{sgn}(\beta)\frac{d\,Bi}{dz}\int_{z}^{\infty}\Psi_a Ai\,dz\right\}. \quad (57b)$$

Again, integration limits are chosen to ensure that $\eta \to 0$ as $z \to \infty$ and that for $z \to -\infty$, the pattern is a trailing spiral,

$$\eta_a \to i\sqrt{\pi}\left[\int_{-\infty}^{\infty}\Psi_a Ai\,dz\right]\left|\frac{x}{\beta}\right|^{1/4} \exp\left[i\,\mathrm{sgn}(\beta)\left(\frac{2}{3}|\beta x^3|^{1/2} + \frac{\pi}{4}\right)\right], \quad -z \gg 1. \quad (58)$$

However, $\Psi_a(z) \equiv 0$ for $|z| \gtrsim e|\beta|^{1/3}$. Furthermore, $e|\beta|^{1/3} \ll 1$ for $e \ll (h/r)\xi^{-1/3}$, in which case we can write

$$\int_{-\infty}^{\infty}\Psi_a Ai(z)\,dz \approx Ai(0)\int_{-e|\beta|^{1/3}}^{e|\beta|^{1/3}}\Psi_a(z)\,dz = 2e\frac{GM_p}{a\sqrt{\pi}}\left(\frac{a\Omega}{c}\right)|\beta|^{1/3}Ai(0). \quad (59)$$

Equation (58) is to be superimposed on (55) and their sum substituted into (56). This yields a flux $F_A \approx m\pi^2\sigma(\Psi_d + \int_{-\infty}^{\infty}\Psi_a Aidz)^2/|\mathscr{D}|$ and a torque

$$T = -\varepsilon\frac{e^2\sigma}{3}\left(\frac{GM_p}{a\Omega}\right)^2\pi m^2\left(\frac{a\Omega}{c}\right)^2\{\mathscr{F}_a(\xi) - \mathscr{F}_2(0,\xi) + 4\mathscr{F}_0(0,\xi)\}^2, \quad (60)$$

where $\mathscr{F}_a(\xi) = 2(3^{1/3}\Gamma(2/3)\xi^{2/3})^{-1}$, $\Gamma(2/3)$ being the gamma function (see Fig. 4). Since η_d and η_a are coherent, there is significant cross-term interaction between waveforms and their forcing functions. This can be illustrated by examining the fine structure torque density (e.g., Shu *et al.* 1985, Ward 1986),

$$\frac{dT}{dr} = -m\pi\sigma rc^{-2}(\Psi_d + \Psi_a)Im(\zeta_d + \zeta_a), \quad (61)$$

which tells us where the torque is exerted on the disk. There are two self-interaction terms whose disk-integrated torques are of $\mathrm{sgn}(-\varepsilon)$ and two cross-interaction terms of $\mathrm{sgn}[-\varepsilon(4\mathscr{F}_0 - \mathscr{F}_2)]$. Thus, these groups will oppose each other if $4\mathscr{F}_0 - \mathscr{F}_2 < 0$. Indeed, the net torque cancels everywhere if $4\mathscr{F}_0 - \mathscr{F}_2 = -\mathscr{F}_a$, which is also evident from Eq. (60). In this case, a wave disturbance is no longer present and the forced response reduces to

$$\eta_d + \eta_a = \mathrm{sgn}(\beta)\frac{\pi\Psi_d}{|\beta|^{1/3}}\frac{d}{dz}Hi(z). \quad (62)$$

The function $dHi/dz \to 1/\pi z^2$ as $-z \gg 1$ and there is no angular momentum transport.

Torques arising from the product of the whole-disk-forcing function, Ψ_d, with the waveforms are exerted over distances on the order of the first wavelength $\sim O(|\beta|^{-1/3})$,

$$\frac{dT_d}{dr} = -m\pi\sigma rc^{-2}\Psi_d Im(\zeta_d + \zeta_a) = -\varepsilon e^2\left(\frac{T_0}{r}\right)(4\mathscr{F}_0 - \mathscr{F}_2)(\mathscr{F}_a - \mathscr{F}_2 + 4\mathscr{F}_0)|\beta|^{1/3}Ai(z), \quad (63)$$

where we have introduced the shorthand T_0 for the torque-like quantity $(\pi m^2\sigma/3)(GM_p/a\Omega)^2(a\Omega/c)^2$. This whole-disk torque may itself vanish if $\mathscr{F}_2 = 4\mathscr{F}_0$, with the effects of radial and tangential perturbations opposing each other. In this case, only the central annulus acts as a wave source.

Torques given by the product of the annulus-forcing function, Ψ_a, with waveforms are exerted in the central annulus only,

$$\frac{dT_a}{dr} = -m\pi\sigma rc^{-2}\Psi_a Im(\zeta_d + \zeta_a) = -\varepsilon e\left(\frac{T_0}{r}\right)\mathscr{F}_a(\mathscr{F}_a - \mathscr{F}_2 + 4\mathscr{F}_0)\left(\frac{2}{\pi}\sin f_c\right), \quad (64)$$

and are generally stronger than (63) by a factor $O(e^{-1})$. However, because (64) is exerted over a narrow zone, its disk-integrated contribution is $O(e^2)$ and comparable to (63). The strong central torque shows up in the changing form of η_a, which can be written

$$\eta_a = -\frac{\pi}{|\beta|^{1/3}} em \frac{GM_p}{a\sqrt{\pi}} \left(\frac{a\Omega}{c}\right) \mathcal{F}_a \begin{cases} [i + \sqrt{3}\,\mathrm{sgn}(\beta)]Ai'(z), & \text{non-wave side} \\ [i + \sqrt{3} - \pi^{-1}\sqrt{3}(2f_c - \sin 2f_c)]Ai'(0), & \text{central annulus} \\ iAi'(z) + \mathrm{sgn}(\beta)Bi'(z), & \text{wave side,} \end{cases} \quad (65)$$

where $(') \equiv d/dz$ and f_c runs from $(\pi/2)(1 + \mathrm{sgn}(\beta))$ on the wave side to $(\pi/2)(1 - \mathrm{sgn}(\beta))$ on the non-wave side. Written in terms of modulus and phase, $\eta_a(z = \pm e|\beta|^{1/3}) \propto 2Ai'(0) \exp[\pm i(\pi/3)\ \mathrm{sgn}(\beta)]$, which reveals a phase rotation of $2\pi/3 = 120°$ across the annulus.

We also see from Eq. (60) that for $\xi \ll 0$ the bracketed term approaches $\mathcal{F}_2^2 \sim 4/\pi\xi^2$ and T approaches a constant value $T \to -\varepsilon(4/3)e^2\sigma(GM_p/a\Omega)^2(a\Omega/c)^4$. (However, since $m \geq 1$ there is a lower limit to ξ of $c/r\Omega$.)

Substitution of (60) into Eq. (2) yields

$$\left(\frac{1}{e}\frac{de}{dt}\right)^L_{\text{co-orbital},m} = -\frac{\pi}{3} m\mu\Omega_p \left(\frac{\sigma a^2}{M_\odot}\right)\left(\frac{a\Omega}{c}\right)^2 \{\mathcal{F}_a(\xi) - \mathcal{F}_2(0, \xi) + 4\mathcal{F}_0(0, \xi)\}^2. \quad (66)$$

Both inner and outer co-orbital resonances *damp* the eccentricity in opposition to Eq. (29). These expressions differ only in their final bracketed quantities which are compared in Fig. 6. For most ξ (and m) the damping of (65) dominates the excitation of (29).

Corotation resonances. The corotation torque is given by Eq. (9) with $\langle\phi_{m,m}\rangle$ substituted for $\phi_{l,m}$,

$$T_m^C = \frac{4}{3}\pi^2 m\langle\phi_{m,m}\rangle^2 \left[\frac{r}{\Omega}\frac{d}{dr}\left(\frac{\sigma}{\Omega}\right)\right]_{r=a}, \quad (67)$$

which is the form suitable for a Keplerian disk. For $\langle\phi_{m,m}\rangle$ we use (43) and (A3) evaluated at $\gamma_0 = 1$ with terms of order e omitted,

$$T_m^C = \frac{16}{3}\pi \frac{\mathcal{F}_0^2}{m}\left(\frac{GM_p}{a\Omega}\right)^2 \left(\frac{a\Omega}{c}\right)^2 \left[r\Omega \frac{d}{dr}\left(\frac{\sigma}{\Omega}\right)\right]_{r=a}. \quad (68)$$

Unlike Eq. (11) for interior and exterior counterparts, Eq. (68) is zero order in the perturber's eccentricity. These are the strong $l = m$ corotation terms that are present for a circular ($e = 0$) orbit. However, because all such components have a pattern speed equal to the perturber, the first term in Eq. (1) vanishes, leaving only the e^2-term in the bracket and

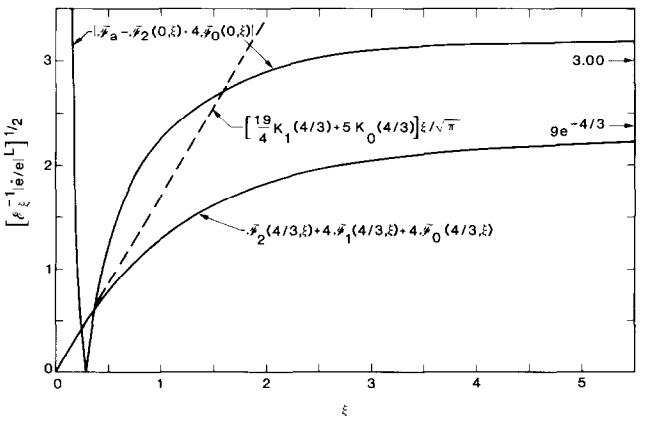

FIG. 6. Eccentricity evolution rates, $|\dot{e}/e|^L$, due to mth-order Lindblad resonances. Rates are normalized to $\mathcal{E}_\xi = (\pi\xi\mu\Omega_p/3)(\sigma a^2/M_\odot)(a\Omega/c)^3$.

$$\left(\frac{1}{e}\frac{de}{dt}\right)^{C}_{\text{co-orbital},m} = \frac{16}{3}\pi\mu\Omega_p\left(\frac{\sigma a^2}{M_\odot}\right)\left(\frac{a\Omega}{c}\right)^2 \left[\frac{d\ln(\sigma/\Omega)}{d\ln r}\right]_{r=a}\frac{\mathcal{F}_0^2(0,\xi)}{m}. \quad (69)$$

The eccentricity may be either excited or damped depending on the sign of the logarithmic derivative. However, if the disk is smoothly varying and the magnitude of the derivative is $\sim O(1)$, (66) exceeds (69) by a factor $\sim O(m^2)$. Thus we expect corotation torques to be less important than Lindblad torques in controlling the eccentricity.

IV. DISCUSSION

It is important to keep in mind that Eqs. (29) and (66) do not actually describe eccentricity variations due to density waves in the solar nebula but refer, instead, to a model problem. Our model is a two-dimensional sheet perturbed by a vertically averaged potential function. It is unavoidable that important features of the disk's behavior will be lost by this approach, especially those involving vertical motions and the development of nonlinear shocks. Nevertheless, our problem is tractable with only a slight modification of standard techniques and, hopefully, preserves enough of the essential elements of the interaction to provide some useful insight. At the very least, it furnishes a reference calculation against which three-dimensional modeling efforts can be compared.

Treating a disk as two-dimensional is only justified if the length scale of the disturbance is long compared to the scale height and its Doppler-shifted frequency is less than the reciprocal of the vertical transit time for sound, $\sim c/h \sim \Omega$. Although the second criterion is generally fulfilled for corotation resonances whose Doppler-shifted frequencies approach zero, it is marginal at best for Lindblad resonances in a non-self-gravitating disk. The azimuthal wavelength of an mth-order potential term is $\gtrsim O(h)$ for $\xi \lesssim O(1)$, $m \lesssim O(r/h)$. For higher order resonances the Laplace coefficients fall off rapidly with height so that a thin layer of material with $z \lesssim r/m$ experiences much stronger forcing than the rest of the column. Vertical averaging tends to smooth this out, a process that becomes increasingly artificial as $m \to \infty$. It seems likely that torques are underestimated generally but that this error is more serious for co-orbital resonances, which have already been found dominant. For instance, one can examine the extreme opposite behavior and assume that there is no vertical communication in the disk, with each layer, $\delta\sigma = \rho\delta z$, responding to its local forcing independently. The total torque would then be found by summing the torques on each layer. This procedure is straightforward for corotation torques and results in replacing $\langle\phi_{m,m}\rangle^2$ with $\langle\phi^2_{m,m}\rangle$ in Eq. (67). For a co-orbital resonance with $\xi \gg 1$, $\langle K_0(z)\rangle^2 \to \pi/\xi^2$ while $\langle K_0^2(z)\rangle \to \pi^{3/2}/2\xi$ (Appendix B). Hence, averaging the potential first results in a smaller torque by a factor $\sim O(\xi^{-1})$. On the other hand, if forcing becomes too pronounced in a thin layer at midplane, the density perturbation ρ' may become comparable to the ambient density ρ and shocks will develop. This in turn will limit the torque so that treating the disk as composed of independent layers probably overestimates the torque.

In any case, we expect all torques to fall off rapidly as $\xi > 1$ from torque cutoff effects (GT80) and the major contributors to eccentricity change will be terms with $\xi \sim O(1)$, $m \sim O(r/h)$. The azimuthal spacing between crests of the spiral wave pattern from these terms will be of order $\sim h$ and the perturber interacts strongly with disk material at this range. At a distance, $|\mathbf{r} - \mathbf{r}_p| = h$, the value of the actual potential, $V = -GM_p/|\mathbf{r} + z\mathbf{k} - \mathbf{r}_p|$, through the disc (i.e., $-h < z < h$) differs by only ~16–17% from its average (Ward 1986), $\langle V\rangle = -(GM_p/h\sqrt{\pi})\exp(|\mathbf{r} - \mathbf{r}_p|^2/2h^2)K_0(|\mathbf{r} - \mathbf{r}_p|^2/2h^2)$.

With these caveats in mind, our analysis suggests several observations regarding the effects of disk–planet tidal interactions on the orbital eccentricity of a perturber. Among those that seem relatively firm are:

(i) Past calculations of eccentricity damping rates are valid only when applied to disk material lying outside the torque cutoff zone, i.e., at a distance greater than the disk's scale height. (ii) If the perturber is embedded in a smooth disk and is of insufficient mass to either open a gap or otherwise seriously distort the local disk structure, corotation torques lying interior to the orbit largely cancel the eccentricity effects of those lying exterior to the orbit. However, Lindblad resonances in both these regions of the disk excite the perturber's eccentricity. (iii) If disk material resides in the orbit of the perturber, strong co-orbital resonances come into play. These consist of both Lindblad and corotation types. (iv) All co-orbital Lindblad resonances damp the eccentricity while corotation torques excite or damp e depending on the sign of the derivative $d(\sigma/B)/dr$. (v) Co-orbital, corotation torques are zero order in e and thus stronger than Lindblad torques, which are order e^2. However, since their pattern speed equals the perturber's mean motion, the ability of corotation torques to alter the eccentricity is reduced. Indeed, if the surface density of the disk varies over a distance long compared to the scale height, Lindblad resonances dominate corotation resonances in the eccentricity variation.

The ultimate outcome will thus depend on a competition between co-orbital Lindblad resonances which damp e and their more distant interior and exterior counterparts which excite e. That these groups oppose each other and are of comparable strength can be regarded as the principal demonstration of this paper. In a sense, this also puts us out of business because, as stressed in Section II, a reliable differencing of two nearly equal rates requires very careful determination of their values. However, we have used our model problem to obtain crude estimates of these torques and the cumulative eccentricity variation rates found by integrating Eqs. (29) and (66) over m are shown in Fig. 7. Both rates are expected to be truncated for $\xi \gtrsim O(1)$ by torque cutoff effects. If effective truncation points, ξ_{max}, are nearly equal, eccentricity damping should prevail for our model problem. Caution is advised, however, since explicit cutoff functions are lacking. Their behavior as well as a realistic treatment of disk thickness may be necessary before this issue can be resolved with complete confidence.

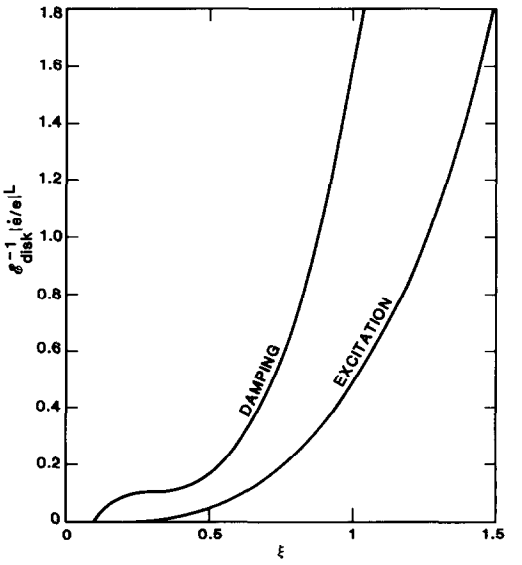

FIG. 7. Cumulative eccentricity evolution rates due to Lindblad torques, $|\dot{e}/e|$, vs ξ. Interior and exterior resonances excite, while co-orbital resonances damp the eccentricity. Rates are normalized to $\mathscr{C}_{disc} = (\pi\mu\Omega_p/3)(\sigma a^2/M_\odot)(a\Omega/c)^4$.

APPENDIX A

The coefficients $\{A_k\}$ are given by

$$A_k = \frac{2}{\sqrt{\pi}} \int_0^\infty \left(-\frac{GM_p}{r_p}\right) \langle b_{1/2}^m \rangle \cos kf \, df, \tag{A1}$$

where

$$\langle b_{1/2}^m \rangle \approx \frac{2}{\sqrt{\pi}} \xi^{-1} \left[\mathcal{F}_0(0, \xi) - m|1 - \gamma| + \frac{1}{2} m^2 \mathcal{F}_2(0, \xi)(1 - \gamma)^2 + \cdots \right]. \quad \text{(A2)}$$

Variations in r_p that are not in the combination $1 - \gamma$ are ignored. This normalized distance to the perturber will go through zero if $|1 - \gamma_0|/\gamma_0 < e$. Inside this range, let f_c be the critical angle for which $1 - \gamma = 0$. Then $e\gamma_0 \cos f_c = 1 - \gamma_0$ and $1 - \gamma = e\gamma_0(\cos f_c - \cos f)$. For $f \lesseqgtr f_c$, $1 - \gamma \lesseqgtr 0$ and integrations involving $\operatorname{sgn}(1 - \gamma)$ must be broken into two parts. Finally, for distances inside (outside) the perturber's perihelion (aphelion), $(1 - \gamma_0)/\gamma_0 \gtrless e$ and we set $f_c = 0(\pi)$. This procedure gives

$$\begin{aligned} A_0 = &- \frac{4GM_p}{\pi h \sqrt{\pi}} \xi^{-1} \left\{ \pi \mathcal{F}_0 + me\gamma_0 \int_0^\infty (\cos f_c - \cos f) df - me\gamma_0 \int_0^\infty (\cos f_c - \cos f) df \right. \\ &\left. + \frac{1}{2} (me\gamma_0)^2 \mathcal{F}_2 \int_0^\infty (\cos^2 f_c - 2 \cos f_c \cos f + \cos^2 f) df \right\} \\ = &- \frac{4GM_p}{\pi r_p \sqrt{\pi}} \xi^{-1} \left\{ \pi \mathcal{F}_0 - me\gamma_0 [(\pi - 2f_c) \cos f_c + 2 \sin f_c] \right. \\ &\left. + \frac{\pi}{2} (me\gamma_0)^2 \mathcal{F}_2 \left(\frac{1}{2} + \cos^2 f_c \right) \right\}. \quad \text{(A3)} \end{aligned}$$

Similarly,

$$A_1 = - \frac{4GM_p}{\pi r_p \sqrt{\pi}} \xi^{-1} \left\{ \frac{1}{2} me\gamma_0 (\pi - 2f_c + \sin 2f_c) - \frac{\pi}{2} (me\gamma_0)^2 \mathcal{F}_2 \cos f_c \right\}, \quad \text{(A4)}$$

and

$$A_2 = - \frac{4GM_p}{\pi r_p \sqrt{\pi}} \xi^{-1} \left\{ me\gamma_0 \sin f_c \left(\cos 2f_c + \frac{2}{3} \sin^2 f_c \right) + \frac{\pi}{8} (me\gamma_0)^2 \mathcal{F}_2 \right\}. \quad \text{(A5)}$$

The coefficients $\{B_k\}$ are given by

$$B_k = \frac{2}{\pi} \int_0^\pi \left(- \frac{GM_p}{r_p} \right) \frac{d}{dr} \langle b_{1/2}^m \rangle \cos kf \, df, \quad \text{(A6)}$$

where

$$r \frac{d}{dr} \langle b_{1/2}^m \rangle \approx \frac{2}{\sqrt{\pi}} h^{-1} [\operatorname{sgn}(1 - \gamma) - m \mathcal{F}_2 (1 - \gamma) + \cdots]. \quad \text{(A7)}$$

Then,

$$\begin{aligned} B_0 = &- \frac{4GM_p}{\pi r_p^2 \sqrt{\pi}} \xi^{-1} m \left\{ - \int_0^{f_c} df + \int_{f_c}^\pi df - me\gamma_0 \mathcal{F}_2 \int_0^\pi (\cos f_c - \cos f) df \right\} \\ = &- \frac{4GM_p}{\pi r_p^2 \sqrt{\pi}} \xi^{-1} m \{ \pi - 2f_c - \pi me\gamma_0 \mathcal{F}_2 \cos f_c \}. \quad \text{(A8)} \end{aligned}$$

Similarly,

$$B_1 = - \frac{4GM_p}{\pi r_p^2 \sqrt{\pi}} \xi^{-1} m \left\{ -2 \sin f_c + \frac{\pi}{2} me\gamma_0 \mathcal{F}_2 \right\}, \quad \text{(A9)}$$

and

$$B_2 = -\frac{4GM_p}{\pi r_p^2\sqrt{\pi}}\,\xi^{-1}m\,\{-\sin 2f_c\}. \tag{A10}$$

To construct $\langle\phi_{m+1,m}\rangle$ and $rd\langle\phi_{m+1,m}\rangle/dr$, we combine $\{A_k\}$, $\{B_k\}$ according to the prescription given (43). If only first-order accuracy is sought, terms to order e in A_1 and B_1 must be kept, but only zero-order terms are needed from the rest. The result is Eqs. (48) and (49) in the text. In Eq. (52), these are further combined to yield the central term on the right-hand side of (45). The remaining forcing terms are $-r^2d^2\langle\phi\rangle/dr^2 + m^2\langle\phi\rangle$. The last of these can be ignored under the same conditions that have been already used to omit a similar term on the left-hand side, i.e., $m \lesssim |\beta|^{1/3}$ (e.g., Goldreich and Tremaine 1979). [Indeed, including such terms when $m \gg |\beta|^{1/3}$ is instrumental in predicting the torque cutoff, but is not addressed here.] By the same argument, all but the first term in $r^2d^2\langle\phi\rangle/dr^2$ can be omitted. However, the delta function must be included in our analysis.

The coefficients $\{C_k\}$ are

$$C_k = \frac{2}{\pi}\int_0^{\pi}\left(-\frac{GM_p}{r_p}\right)\left(-\frac{4}{hr_p\sqrt{\pi}}\right)\delta(1-\gamma)\cos kf\,df. \tag{A11}$$

Let $y = 1 - \gamma = -x - e\gamma_0\cos f$. Then $\cos f = -(x+y)/e\gamma_0$, $df = dy/\sqrt{(e\gamma_0)^2 - (x+y)^2}$, and

$$C_0 = \frac{8GM_p}{\pi r_p^2 h\sqrt{\pi}}\int_{-x-e\gamma_0}^{-x+e\gamma_0}\frac{\delta(y)\,dy}{\sqrt{(e\gamma_0)^2-(x+y)^2}} = \frac{8GM_p}{\pi r_p^2 h\sqrt{\pi}}\frac{1}{\sqrt{(e\gamma_0)^2-x^2}}. \tag{A12}$$

Similarly,

$$C_1 = \frac{8GM_p}{\pi r_p^2 h\sqrt{\pi}}\int_{-x-e\gamma_0}^{-x+e\gamma_0} -\left(\frac{x+y}{e\gamma_0}\right)\frac{\delta(y)\,dy}{\sqrt{(e\gamma_0)^2-(x+y)^2}} = -\frac{8GM_p}{\pi r_p^2 h\sqrt{\pi}}\frac{(x/e\gamma_0)}{\sqrt{(e\gamma_0)^2-x^2}}, \tag{A13}$$

and

$$C_2 = \frac{8GM_p}{\pi r_p^2 h\sqrt{\pi}}\int_{-x-e\gamma_0}^{-x+e\gamma_0}\left[2\left(\frac{x+y}{e\gamma_0}\right)^2 - 1\right]\frac{\delta(y)\,dy}{\sqrt{(e\gamma_0)^2-(x+y)^2}} = \frac{8GM_p}{\pi r_p^2 h\sqrt{\pi}}\frac{2(x/e\gamma_0)^2-1}{\sqrt{(e\gamma_0)^2-x^2}}. \tag{A14}$$

These expressions are valid only if $|x| < e\gamma_0$, otherwise they are zero. All three coefficients are $\propto e^{-1}$; hence, to the lowest order we need only retain the middle term in the C_k-version of (44), i.e.,

$$r^2\frac{d^2}{dr^2}\langle\phi_{m\pm1,m}\rangle \approx \frac{1}{2}r^2C_1 \approx -\frac{4GM_p}{\pi h\sqrt{\pi}}\frac{\cot f_c}{e\gamma_0}, \tag{A15}$$

where we have replaced $x = -e\gamma_0\cos f_c$ and $\sqrt{(e\gamma_0)^2 - x^2} = e\gamma_0\sin f_c$.

APPENDIX B

To compute the vertical average of $K_0^2(t)$, the integral representation

$$K_0(t) = \int_0^{\infty}\frac{\cos(tx)\,dx}{\sqrt{x^2+1}} \tag{B1}$$

is employed in the averaging integral

$$\langle K_0^2 \rangle = \frac{2}{\sqrt{\pi}\,\xi} \int_0^\infty e^{-(t/\xi)^2} K_0^2(t)\, dt$$

$$= \frac{2}{\sqrt{\pi}\,\xi} \int_0^\infty e^{-(t/\xi)^2} \left[\int_0^\infty \frac{\cos(tx)\, dx}{\sqrt{x^2+1}} \right] \left[\int_0^\infty \frac{\cos(tx')\, dx}{\sqrt{x'^2+1}} \right] dt \quad \text{(B2)}$$

$$= \frac{1}{\sqrt{\pi}\xi} \int_0^\infty dx \int_0^\infty dx' \frac{1}{\sqrt{(x^2+1)(x'^2+1)}} \int_0^\infty dt\, e^{-(t/\xi)^2} [\cos t(x+x') + \cos t(x-x')],$$

where the order of integration has been reversed and the cosine product written as a sum of cosines. The t-integral is

$$\int_0^\infty dt\, e^{-(t/\xi)^2} \cos t(x \pm x')\, dt = \frac{\sqrt{\pi}}{2} \xi e^{-[\xi(x \pm x')/2]^2}, \quad \text{(B3)}$$

and

$$\langle K_0^2 \rangle = \frac{1}{2} \int_0^\infty dx \int_0^\infty dx' \frac{e^{-[\xi(x+x')/2]^2} + e^{-[\xi(x-x')/2]^2}}{\sqrt{(x^2+1)(x'^2+1)}}. \quad \text{(B4)}$$

We extend integration limits to $(-\infty, \infty)$, divide by 4 to compensate, and change variables to $y = x + x'$, $z = x - x'$,

$$\langle K_0^2 \rangle = \frac{1}{8} \int_{-\infty}^\infty dz \int_{-\infty}^\infty dy \left| \frac{\partial(x, x')}{\partial(y, z)} \right| \left\{ \frac{e^{-(\xi y/2)^2} + e^{-(\xi z/2)^2}}{[(y+z)^2/4 + 1]^{1/2}[(y-z)^2/4 + 1]^{1/2}} \right\}. \quad \text{(B5)}$$

By symmetry arguments, both exponentials contribute equal amounts,

$$= \frac{1}{2\xi} \int_{-\infty}^\infty dz \int_{-\infty}^\infty \xi \frac{e^{-(\xi y/2)^2}\, dy}{[(y+z)^2 + 4]^{1/2}[(y-z)^2 + 4]^{1/2}}. \quad \text{(B6)}$$

We have included ξ in both numerator and denominator in Eq. (B6). Now let $\xi \to \infty$, and identify $\xi \exp[-(\xi y/2)^2] \to 2\sqrt{\pi}\delta(y)$, $\delta(y)$ being the delta function. Then

$$\langle K_0^2 \rangle \to \frac{\sqrt{\pi}}{\xi} \int_{-\infty}^\infty \frac{dz}{\sqrt{z^2+4}} = \frac{\pi\sqrt{\pi}}{2\xi}. \quad \text{(B7)}$$

ACKNOWLEDGMENTS

The author thanks Dr. F. H. Shu and an anonymous referee for several valuable comments and the Department of Physics, Harvey Mudd College, for its hospitality during a portion of this research project. Useful discussions with Dr. P. Goldreich at an earlier stage of this work are also acknowledged. This research was supported by NASA under Contract NBAS7-100 with the Jet Propulsion Laboratory, California Institute of Technology.

REFERENCES

ABRAMOWITZ, M., AND I. A. STEGUN 1968. *Handbook of Mathematical Functions,* National Bureau of Standards, U.S. Government Printing Office, Washington, D.C.

ADACHI, I., C. HAYASHI, AND K. NAKAZAWA 1976. The gas drag effect on the elliptic motion of a solid body in the primordial solar nebula. *Prog. Theor. Phys.* **56,** 1756–1771.

BORDERIES, N., P. GOLDREICH, AND S. TREMAINE 1984. Excitation of inclinations in ring–satellite systems. *Astron. J.* **284,** 429–434.

BROUWER, D., AND CLEMENCE, G. M. 1961. *Methods of Celestial Mechanics,* p. 598. Academic Press, New York.

DONNER, K. 1978. Ph.D. thesis, University of Cambridge.

GOLDREICH, P., AND S. TREMAINE 1978. The formation of the Cassini division in Saturn's rings. *Icarus* **34,** 240–253.

GOLDREICH, P., AND S. TREMAINE 1979. The excitation of density waves at the Lindblad and corotation resonances by an external potential. *Astrophys. J.* **233,** 857–871.

GOLDREICH, P., AND S. TREMAINE 1980. Disk–satellite interaction. *Astrophys. J.* **241,** 425–441.

GOLDREICH, P., AND S. TREMAINE 1981. The origin of the eccentricities of the rings of Uranus. *Astrophys. J.* **243,** 1062–1075.

HOURIGAN, K., AND W. R. WARD 1984. Radial migration of preplanetary material: Implications for the accretion time scale problem. *Icarus* **60,** 29–39.

LIN, D. N. C., AND J. PAPALOIZOU 1979. Tidal torques on accretion discs in binary systems with extreme mass ratios. *Mon. Not. R. Astron. Soc.* **186,** 799–812.

LIN, D. N. C., AND J. PAPALOIZOU 1986. On the tidal interaction between protoplanets and the primordial solar nebula. II. Self-consistent nonlinear interaction. *Astrophys. J.* **307,** 395–409.

LISSAUER, J. J., F. H. SHU, AND J. N. CUZZI 1981. Moonlets in Saturn's ring? *Nature* **292,** 707–711.

LYNDEN-BELL, D., AND A. J. KALNAJS 1972. On the generating mechanism of spiral structure. *Mon. Not. R. Astron. Soc.* **157,** 1–30.

NAKANO, T. 1987. The formation of planets around stars of various masses and the origin and the evolution of circumstellar dust clouds. In *Star Forming Regions,* IAU symposium No. 115.

PAPALOIZOU, J., AND D. N. C. LIN 1984. On the tidal interaction between protoplanets and the primoridal solar nebula. I. Linear calculation of the role of angular momentum exchange. *Astrophys. J.* **285,** 818–834.

SAFRONOV, V. S. 1972. *Evolution of the Protoplanetary Cloud and the Earth and Planets* (Transl. Israel Program for Scientific Translation, NASA TTF-677). Nauka, Moscow.

SHU, F. H. 1984. Waves in planetary rings. In *Planetary Rings* (Greenberg and Brahic, Eds.), pp. 513–561. Univ. of Arizona Press, Tucson.

SHU, F. H., C. YUAN, AND J. J. LISSAUER 1985. Nonlinear spiral density waves: An invicid theory. *Astrophys. J.* **291,** 356–376.

WARD, W. R. 1986. Density waves in the solar nebula: Differential Lindblad torque. *Icarus* **67,** 164–180.

WEIDENSCHILLING, S. J. 1977. Aerodynamics of solid bodies in the solar nebula. *Mon. Not. R. Astron. Soc.* **180,** 57–70.

WETHERILL, G. W. 1980. Formation of terrestrial planets. *Annu. Rev. Astron. Astrophys.* **18,** 77–113.

WHIPPLE, F. 1972. On certain aerodynamic processes for asteroids and comets. In *From Plasma to Planet* (A. Elvins, Ed.), pp. 211–232. Wiley, New York.